The 8th International Supercritical CO_2 Power Cycles Symposium
February 27 – 29, 2024, San Antonio, Texas
Paper #67

Heat Transfer Experiments of Ribbed, Serpentine Cooling Passages with Supercritical CO_2

Michael Marshall
Research Engineer
Southwest Research Institute
San Antonio, TX

Mark Anguiano
Research Engineer
Southwest Research Institute
San Antonio, TX

Jeffrey Moore, Ph.D.
Institute Engineer
Southwest Research Institute
San Antonio, TX

Michael Marshall is a Research Engineer in the Machinery Department at Southwest Research Institute, where he has conducted work on a range of sCO2 power cycle applications. He earned his Bachelors in Aerospace Engineering in 2018 from the University of Virginia. His past experience includes experimental heat transfer testing, turbomachine and heat exchanger design, root cause failure analysis, and thermodynamic cycle modeling.

Mark Anguiano is a Research Engineer in the Machinery Department at Southwest Research Institute. His research experience includes the design and testing of components such as dry gas seals and cryogenic pumps. He has also designed test loops and ancillary systems (lube oil, dry gas seal) for turbine and compressor powertrains. Mr. Anguiano earned his Bachelor of Science degree in Mechanical Engineering from the University of Texas at San Antonio and is currently pursuing a Master of Science degree.

Dr. Jeffrey Moore is an Institute Engineer in the Machinery Section at Southwest Research Institute in San Antonio, TX. He holds a B.S., M.S., and Ph.D. in Mechanical Engineering from Texas A&M University. His professional experience over the last 30 years includes engineering and management responsibilities related to centrifugal compressors and gas turbines at Solar Turbines Inc. in San Diego, CA, Dresser-Rand (now Siemens Energy) in Olean, NY, and Southwest Research Institute in San Antonio, TX. His interests include advanced power cycles and compression methods, rotordynamics, seals and bearings, computational fluid dynamics, finite element analysis, machine design, controls, aerodynamics, and oxy-combustion. He has authored over 40 technical papers related to turbomachinery and has four patents issued. Dr. Moore has held positions as the Vanguard Chair of the Structures and Dynamics Committee and Chair of Oil and Gas Committee for IGTI Turbo Expo. He has also served as the Associate Editor for the Journal of Tribology and a member of the IGTI sCO2 Committee, Turbomachinery Symposium Advisory Committee, the IFToMM International Rotordynamics Conference Committee, and the API 616 and 684 Task Forces.

ABSTRACT

The results of heat transfer experiments with supercritical CO_2 (sCO_2) to capture the performance of ribbed, serpentine cooling passages for Reynolds numbers in the range of 100,000 - 400,000 are presented. The oxy-combustion turbine operating in an Allam-Fetvedt cycle has a turbine inlet temperature exceeding 1100°C, necessitating internally cooled turbine blades due to material creep strength limits. Reynolds numbers for sCO_2, with its combination of high fluid density and low viscosity, can be up to an order of magnitude higher than comparable internal cooling conditions for an air-breathing engine where the majority of experimental data exists. To improve the prediction of cooling performance through turbulated passages, a test rig was designed and constructed with interchangeable insert capability for operation in sCO_2 with heat transfer from a heater outlet flow stream to a lower temperature recuperator outlet flow stream. The inserts included serpentine passage geometry with five passes, one of the inserts including chevron ribs and the other a plain wall. The multi-pass serpentine geometry allowed for the evaluation of the effects 180 deg. tip turns have on the return passage flow characteristics, as they can depart significantly from fully-developed flow characteristics. The test procedure included the use of a modified Wilson plot method, with hot flow stream conditions kept effectively constant so that monitored changes in the overall thermal resistance could be attributed to manipulations in cooling flow stream conditions. Conditions during testing consisted of test section pressures of approximately 180 bar, cooling flow stream temperature of 175°C and hot flow stream temperature of 410°C. Test points at discrete cool flow Reynolds numbers up to 400,000 demonstrated an expected trend of decreased fluid thermal resistance with increasing Reynolds number, while at comparable Reynolds number there was an exhibited lower thermal resistance and higher passage pressure drop for the ribbed insert compared to the plain-walled insert. Processing of test data included establishment of Nusselt number enhancement ratios, so that for different internal cooling passage dimensions in the actual turbine blade at comparable Reynolds number the ratio could be applied to predict cooling performance.

INTRODUCTION

Direct-fired sCO_2 power cycles featuring oxy-combustion are a promising technology due to the ability to have near zero CO_2 emissions while achieving competitive plant efficiencies on the utility scale. Past system studies on the Allam-Fetvedt cycle predicted a 53% LHV net efficiency for a plant utilizing natural gas [1], and a 42% LHV net efficiency for a plant utilizing coal syngas fuel [2]. These systems rely on a sCO_2 turbine operating with turbine inlet temperatures exceeding 1100°C. The turbine blade cooling scheme identified to be necessary for the application is similar to that seen in typical gas turbine blades including impingement cooling in the leading edge region, serpentine cooling in the blade mid-section, and pin-fin cooling in the trailing edge region. Previously, experimental work completed under the same syngas oxy-combustion turbine development project sponsored by the U.S. Department of Energy (FE-0031929) included pin-fin array and jet impingement tests with sCO_2 [3, 4]. For mid-section cooling passage geometries, there are a plethora of experimental studies with air that provide data on Nusselt number enhancement ratios (Nu/Nu_0) and friction factor ratios (f/f_0). These particular ratios are of great convenience when designing the turbine blade for end application, as the smooth wall values can be readily calculated based on literature correlations with the known blade internal geometry and local fluid thermodynamic properties. In a study by Wright et al. [5] including multiple aspect ratios and rib geometries, trends of a slight decrease in Nu/Nu_0 with increasing Reynolds number up to 40,000 were seen. While most studies involving air have Reynolds number below 100,000, Wieler et al. [6] conducted a study of a ribbed channel going up to a Reynolds number of 142,000, while demonstrating that there can be noticeable variation

in Nu/Nu_0 along the length of a ribbed passage with the highest values found in the developing flow region. Test data also demonstrates that the 180 deg. tip turn between neighboring passages is the source of locally higher Nusselt numbers as well as significant pressure drop that can be 2 times the local fluid dynamic pressure [7]. With the high density of CO_2 in its supercritical state with turbine inlet pressures above 300 bar, cooling flow Reynolds numbers can regularly be in the range between 100,000 and 400,000. Testing with sCO_2 in this flow regime was conducted by Searle et al. [8], observing that an angled ribbed passage at Reynolds number near 140,000 saw a Nu/Nu_0 value between 2.5 and 3.0 and a stable trend and slight increase of Nu/Nu_0 with Reynolds numbers for several passage geometries. The test campaign described in the following sections sought to gain heat transfer data for a geometry that included both ribbed passage lengths with the effect of 180 deg. tip turns, for conditions in sCO_2 that were representative of those to be seen in the end oxy-fuel turbine application.

Test Section and System Design

In order to conduct heat transfer testing with sCO_2, existing equipment was leveraged from a 1 MWe test loop at Southwest Research Institute. A two-stage compressor and loop process cooler were first used as part of a test program for an integrally geared compander supported by the DOE [9]. A natural gas fired primary heater for CO_2 and 3 MWth recuperator were commissioned and tested as part of a sCO_2 turbo-expander development program targeted towards CSP application [10]. This equipment was leveraged in order to supply both hot and cooling flow streams at supercritical conditions for a heat transfer test section. The hot stream comes from the primary heater downstream of the two-stage compressor and the cooling flow comes from the recuperator outlet, bypassing the primary heater. Another flow stream from the discharge of the second stage compressor is introduced downstream of the test section to further decrease the bulk flow temperature to stay within downstream equipment ratings. The process & instrumentation diagram (P&ID) for the test section can be seen in Figure 1, with the physical layout seen in Figure 2.

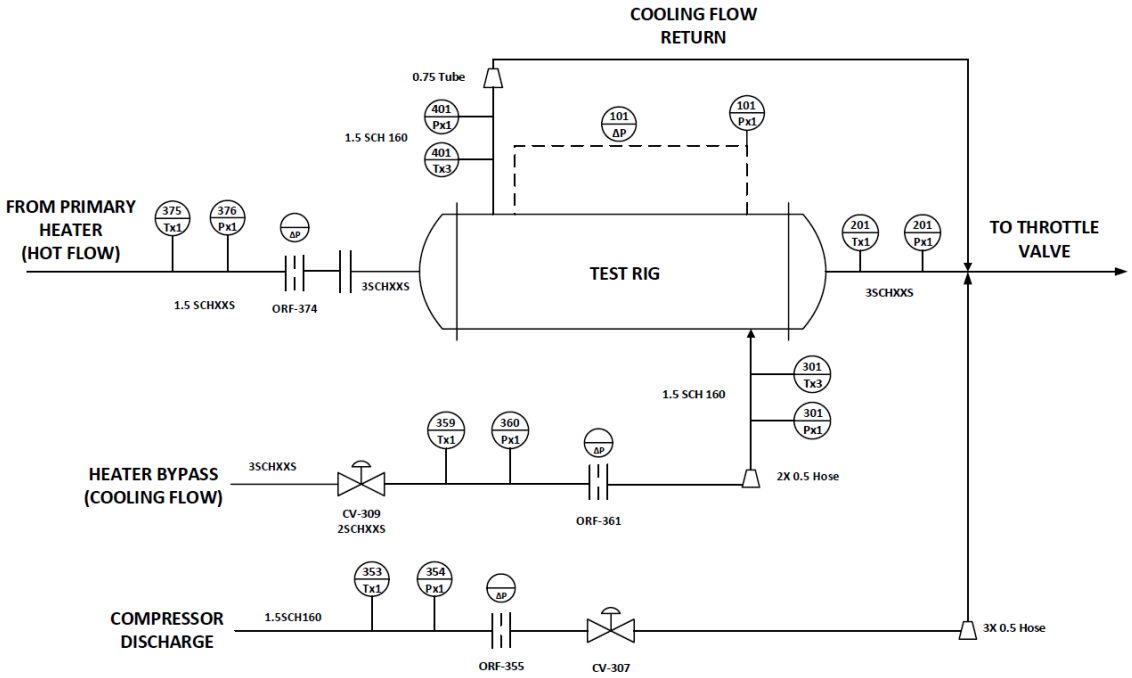

Figure 1. P&ID of flow streams utilized from main sCO_2 test loop for heat transfer testing.

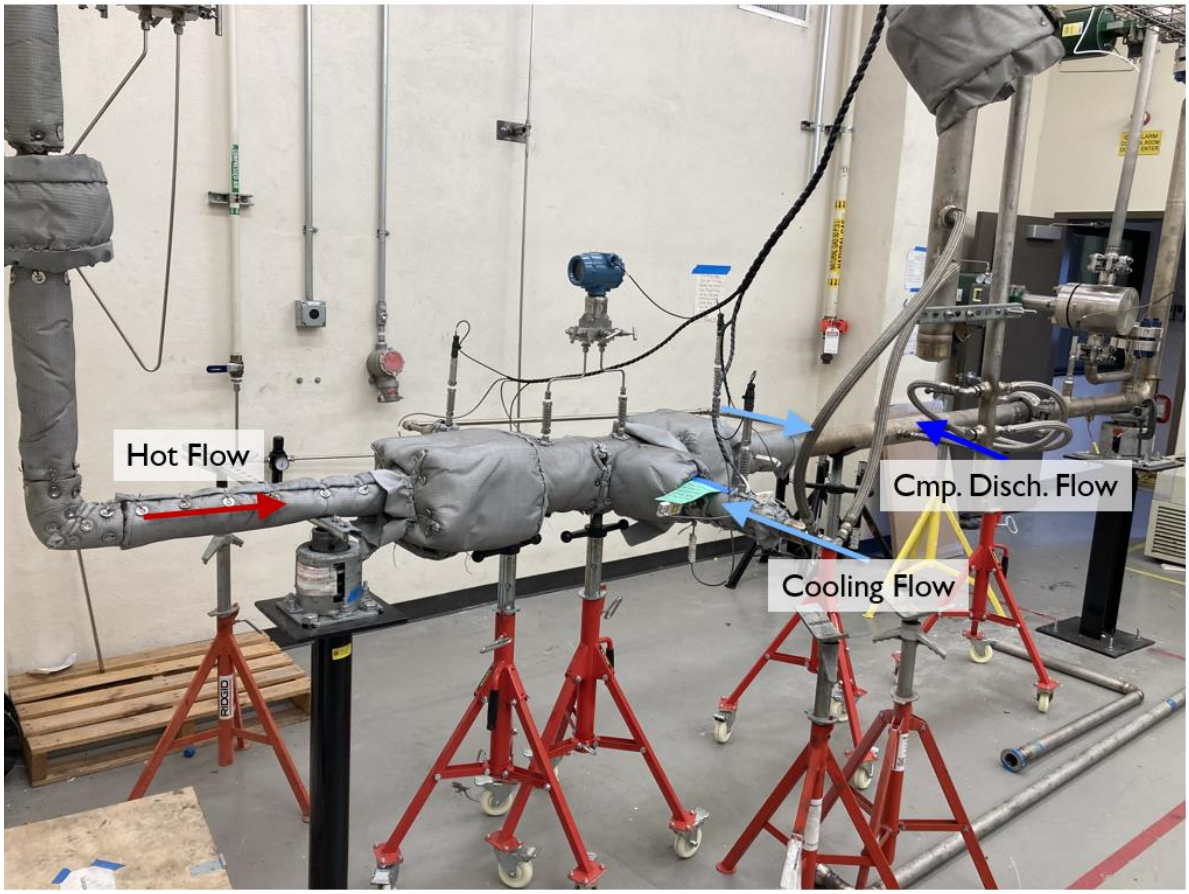

Figure 2.Physical orientation of flow sources from the sCO_2 test loop with the heat transfer test section seen insulated at center.

The test section was designed around the need to represent the mid-section serpentine cooling geometry. To do this it was conceived to have the hot flow through a tubular insert, with the cooling flow in an annular flowpath along the outside of the insert all inside a case purposed for pressure containment. The outside of the tubular insert features two symmetric flow serpentine pathways, each with five passes. This flowpath was machined from 316 stainless steel bar stock (Figure 3), with the dimensions enumerated in Table 1 following common standard design practice and those expected for the blade application.

Figure 3. Machined flowpath for cooling flow featuring chevron ribs. At center is shown the terminating passage of the two symmetric, serpentine flowpaths.

Table 1. Parameters of ribbed test section flowpath seen in Figure 3. Parameters for the rib height and rib pitch ratios were based on common design practice referenced in data from Han [7], while the length to diameter ratio is based on expected turbine first stage blade dimensions.

Parameter	Value
Rib height to hydraulic diameter (e/D_h)	0.076
Rib pitch to rib height (p/e)	10
Rib chevron (V) angle	45 deg.
Passage length to hydraulic diam. ratio (L/D_h)	10
Passage aspect ratio (w/h)	1

It was noted that the test geometry was only capable of ribs on only one passage wall as opposed to two walls as would be the case in a blade passage. To account for this, the passage aspect ratio for the insert was chosen to simulate half the height of an expected midsection blade passage. Work from Rau et al. [11] motivated the use of a half passage height in order to match vortical structures, while work from Chandra [12] demonstrated that (Nu/Nu_0) values on a ribbed wall surface are relatively unchanged by whether or not the opposite wall also has ribs.

Another requirement of the test section was that inserts be interchangeable, with a test employing the serpentine passage design without chevron ribs conducted in addition to the insert with ribs. To facilitate this, a custom seal ring for the clamp style flange connector was procured that included holes which seal inserts on either end of the case were bolted to. Between these seal inserts, the main insert (Figure 4) could be supported while allowing for thermal growth. Metallic pressure energized seals were used on the main insert and the seal insert in different locations to seal each possible leakage path between the hot and cooling flow streams. A spring energized PTFE seal was used to seal against the case inner surface, inserted on a sleeve

welded to the outer diameter of the ribbed passage dividing walls. The sleeve and its seal prevented flow from both bypassing the entire serpentine pathway and leaking from one passage to the adjourning one. To assemble the internal components into the casing, a horizontal assembly was employed leveraging an aluminum rod that the stainless steel inserts could slide on before being captured by the seal ring on the opposite end.

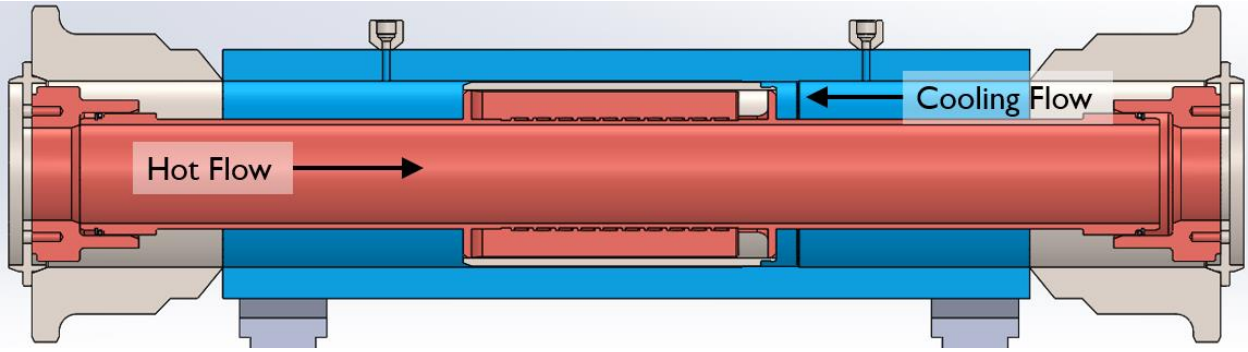

Figure 4. Cross-section solid model of insert and casing geometry. There is a counter-flow orientation based on the inlet and exit port locations of the cooling flow relative to the direction of hot flow.

Figure 5. Internal test section components as seen in Figure 4 at different stages of the assembly process.

The outer case and connected piping and nozzles were all rated to a design pressure of 250 bar and temperature of 537°C to the intent of Section VIII of the ASME Boiler and Pressure Vessel Code (BPVC) [13]. A design-by-analysis approach as outlined in Division 2 was used for the main case due to the multiple welded nozzles present for flow routing and instrumentation. All test rig components underwent hydrostatic pressure tests according to the BPVC before test loop commissioning.

For the test section instrumentation, insulated ports connected to the casing for the inlet and exit cooling flow each included three thermowell mounted RTDs each 90 deg. apart and a single pressure transducer. The port sections were sized to have a velocity under 3 m/s to prevent

significant variation in static temperature on the thermowell surface as can be seen in higher velocity flow. The use of three thermowells was selected so that a faulty RTD could be identified and the average of the three probes could enhance the accuracy of the bulk flow temperature reading. A differential pressure transmitter was mounted with taps immediately upstream and downstream of the serpentine flow path so that the pressure drop could be measured for each test condition. Orifice flow meters were implemented to register the mass flow rates of the respective flow streams, and additional pressure transmitters and thermocouples were used throughout the connected piping to inform valve operation and other loop controls.

DATA REDUCTION METHODS

The overall target of test operation was to collect data at varying Reynolds number for the cooling flow and capture the fluid thermal resistance and pressure drop to be able inform enhancement ratios (Nu/Nu_0) and friction factor ratios (f/f_0). The cooling flow mass flow rate, and therefore Reynolds number, was modified through manipulation of a control valve on that bypass line from the high pressure recuperator stream. To isolate the heat transfer characteristics of the cooling flow, a modified Wilson plot technique was employed similar to the implementation used in sCO_2 heat transfer experiments by Searle et al. [8]. This method, as described further in following paragraphs, required a control strategy that sought to keep the mass flow rate and temperature of the hot flow from the primary heater constant across test points. Key parameters are defined in Eq. 1 – Eq. 3, with the subscript *c* denoting the cooling flow and subscript *h* the hot flow stream. A factor of 2 is included on the denominator for Reynolds number due to the cooling mass flow rate dividing between twin pathways.:

$$RE = \frac{\dot{m}_c D_{passage}}{2\mu(T_c,P_c)A_{passage}} \quad \text{(Eq. 1)}$$

$$R_{total} = \frac{\Delta T_{LMTD}}{q} = \frac{\frac{\left(\left(T_{h,in}-T_{c,out}\right)-\left(T_{h,out}-T_{c,in}\right)\right)}{ln\left(\frac{T_{h,in}-T_{c,out}}{T_{h,out}-T_{c,in}}\right)}}{\dot{m}_c\left(h\left(T_{c,in},P_{c,in}\right)-h\left(T_{c,out},P_{c,out}\right)\right)} \quad \text{(Eq. 2)}$$

$$R_{total} = R_{t,c} + R_{t,w} + R_{t,h} \quad \text{(Eq. 3)}$$

To isolate the cooling flow thermal resistance from the total thermal resistance, the modified Wilson plot method was used leveraging the test points of the smooth wall insert. While hot flow conditions were kept nearly constant, test points were taken and plotted at varying cooling flow Reynolds number with a curve fit applied matching the form in Equation 4.

$$R_{total} = m\left(\frac{1}{Re^{0.8}Pr^{0.4}k}\right) + (R_{const}), of\ form\ y = mx + b \quad \text{(Eq. 4)}$$

m ≡ slope of Wilson plot

$R_{const} = R_{t,w} + R_{t,h}$

The y-intercept (b) indicates the constant thermal resistance (R_{const}) contribution that can be assumed from the hot fluid and wall. For any test point, the Nusselt number can be extracted from the cooling flow thermal resistance contribution through the derivation in Eq. 5 and 6. When calculating the Nusselt number, an effective heat transfer surface area (A_{eff}) must be used. This is due to the fact that the passage dividing walls see a decreasing temperature potential radially outwards from the base metal surface at the tube surface outer diameter. The same situation is

true for the actual turbine blade, as the passage dividing walls see that decreasing temperature potential away from the external blade surface exposed to the main turbine flow path. For the nominal heat transfer surface area used as an input for the effective area calculation, the plain wall insert surface area is used for all calculations for consistency.

$$R_{t,c} = R_{total} - R_{const} = \frac{1}{UA_{eff}} \rightarrow U = \frac{1}{R_{t,c}A_{eff}} \quad \text{(Eq. 5)}$$

$$Nu = \frac{UD_h}{k} \quad \text{(Eq. 6)}$$

In order to find the overall heat transfer coefficient (U) and therefore Nusselt number for any individual test point, an iterative solver is used due to the dependence of A_{eff} on U. The solver employs a discretized model of the passage dividing walls temperature profile. The overall heat transfer coefficient is iterated until convergence according to Eq. 5. The heat transfer balance derivation for the passage walls can be seen in Figure 6 with the resulting matrix formation in Eq. 7 and 8.

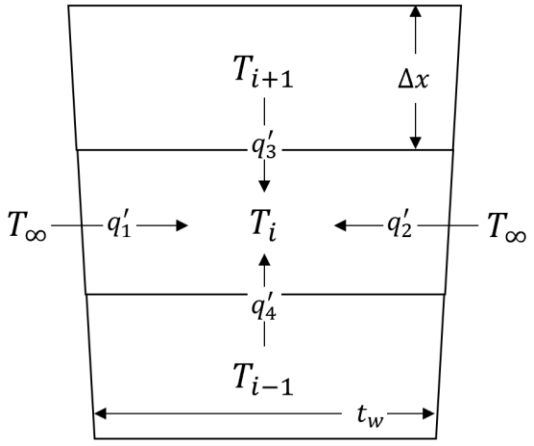

$$q_1' = U\Delta x(T_\infty - T_i)$$
$$q_2' = U\Delta x(T_\infty - T_i)$$
$$q_3' = \frac{kt_w(T_{i+1} - T_i)}{\Delta x}$$
$$q_4' = \frac{kt_w(T_{i-1} - T_i)}{\Delta x}$$

Figure 6. Heat transfer balance in a discretized model of a passage wall between neighboring passes in the serpentine flowpath.

$$\left(\frac{kt_w}{\Delta x}\right)T_{i-1} + \left(-\frac{2kt_w}{\Delta x} - 2U\Delta x\right)T_i + \left(\frac{kt_w}{\Delta x}\right)T_{i+1} = -2U(\Delta x)T_\infty \quad \text{(Eq. 7)}$$

$$\begin{bmatrix} 1 & \cdots & a_{1n} \\ \vdots & \ddots & \vdots \\ a_{n1} & \cdots & a_{nn} \end{bmatrix}\begin{bmatrix} T_1 \\ T_i \\ T_n \end{bmatrix} = \begin{bmatrix} T_{base} \\ b_i \\ b_n \end{bmatrix} \quad \text{(Eq. 8)}$$

For the smooth wall Nusselt number, the Petukhov friction factor equation and Gnielinski Nusselt number correlation are used as found in the text from Incropera et al. [14].

$$f_0 = (0.790\ln(Re) - 1.64)^{-2} \quad \text{(Eq. 9)}$$

$$Nu_0 = \frac{\left(\frac{f_0}{8}\right)(Re-1000)Pr}{1+12.7\left(\frac{f_0}{8}\right)^{\frac{1}{2}}(Pr^{\frac{2}{3}}-1)} \quad \text{(Eq. 10)}$$

The measurement of differential pressure across the serpentine flowpath obfuscates the friction factor as defined in literature as losses result from each 180 deg. flow turn in addition to the straight passage frictional losses. In turn, the following equation is used:

$$k = \frac{\Delta P}{P_{dyn}} \quad \text{(Eq. 11)}$$

$$f = \frac{(\Delta P - 4k_{turn}P_{dyn})D_h}{P_{dyn}L_{total}} \quad \text{(Eq. 12)}$$

$P_{dyn} = \frac{\left(\frac{\dot{m}_c}{2A_{passage}}\right)^2}{2\rho} \equiv$ passage dynamic pressure

$k_{turn} \equiv$ loss factor assumed for each tip turn, four in total.

An uncertainty analysis was completed on reported test points with the intent of the ASME Journal of Heat Transfer guidelines [15], using error propagation methods of bias and precision uncertainty. The bias limit values included instrument uncertainties for multi-point calibrated RTDs and thermocouples, differential pressure transmitters, and orifice plate discharge coefficients. The precision limit values were calculated as two times the standard deviation of the reported variable in the test data that was taken at 1-second intervals, for a total of 30 samples for each data point. This precision limit accounts for the unsteadiness in process variables during each 30-second average taken for a test point. While a constant thermal resistance component was assumed through the modified Wilson plot method in order to calculate the cooling flow thermal resistance for each test point, there was naturally some variation in the hot stream mass flow rate and temperature. In order to account for the impact that has on the uncertainty of the cooling flow thermal resistance, two-times the standard deviation of the estimated hot flow heat transfer coefficient using the Dittus-Boelter correlation across test data was implemented into an error propagation equation for calculation of cooling flow thermal resistance.

RESULTS AND DISCUSSION

To reach planned testing conditions, the test loop was purged and the startup procedure of the compressor begun once first stage suction conditions were in the supercritical phase. As the compressor reached full speed, the natural gas flow to the primary heater was increased gradually in order to raise the CO_2 outlet temperature. The temperature for the hot flow to the test section was raised at a rate of approximately 60°C per hour, until reaching a temperature of just over 400°C where test points were taken. The range of pressure and temperature state points for each of the streams for reported test points are enumerated in Table 2.

Table 2. Range of pressure, temperature, and flow rates for hot and cooling flow streams for reported test points.

Parameter	Minimum value	Maximum value
Cooling Flow Inlet Pressure (bar)	183	205
Hot Flow Inlet Pressure (bar)	184	205
Cooling Flow Inlet Temperature (°C)	165	192
Cooling Flow Outlet Temperature (°C)	209	239
Hot Flow Inlet Temperature (°C)	402	418
Cooling Flow Mass Flow Rate (kg/s)	0.108	0.380
Hot Flow Mass Flow Rate (kg/s)	1.43	1.49

One of the main considerations regarding test section conditions was to minimize uncertainty. This was done by targeting inlet state points above 150°C for a lower specific heat than the maximum seen at lower temperatures at a 200 bar isobar, and maintaining a temperature difference between the two streams of approximately 200°C to generate a significant temperature delta across the test section.

Between test points when valve controls were manipulated to reach a new target Reynolds number, real-time charts in the LabVIEW program were monitored to judge the arrival at a quasi-steady-state test point. When charts of cooling flow inlet temperature and total thermal resistance were observed to oscillate around a near constant value, a 30 second averaging of the data was taken and registered as a test point. With each adjustment in loop controls to arrive at a new Reynolds number, typical spans of 10-15 minutes were used between the registering of test points. Data points registered and plotted for total thermal resistance across the test section, the Nusselt number, Nusselt number enhancement ratio, and friction factor enhancement ratio are seen in Figures 7-10.

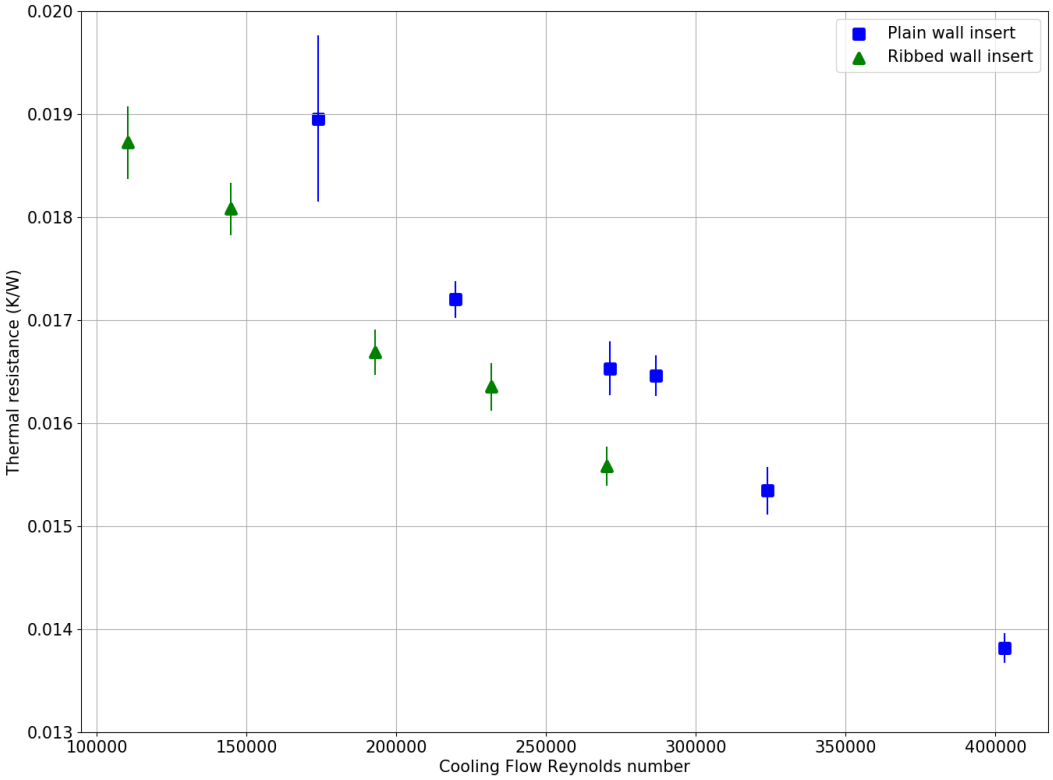

Figure 7. Total thermal resistance measured across the test section for plain and ribbed wall inserts over a range of cooling flow Reynolds numbers.

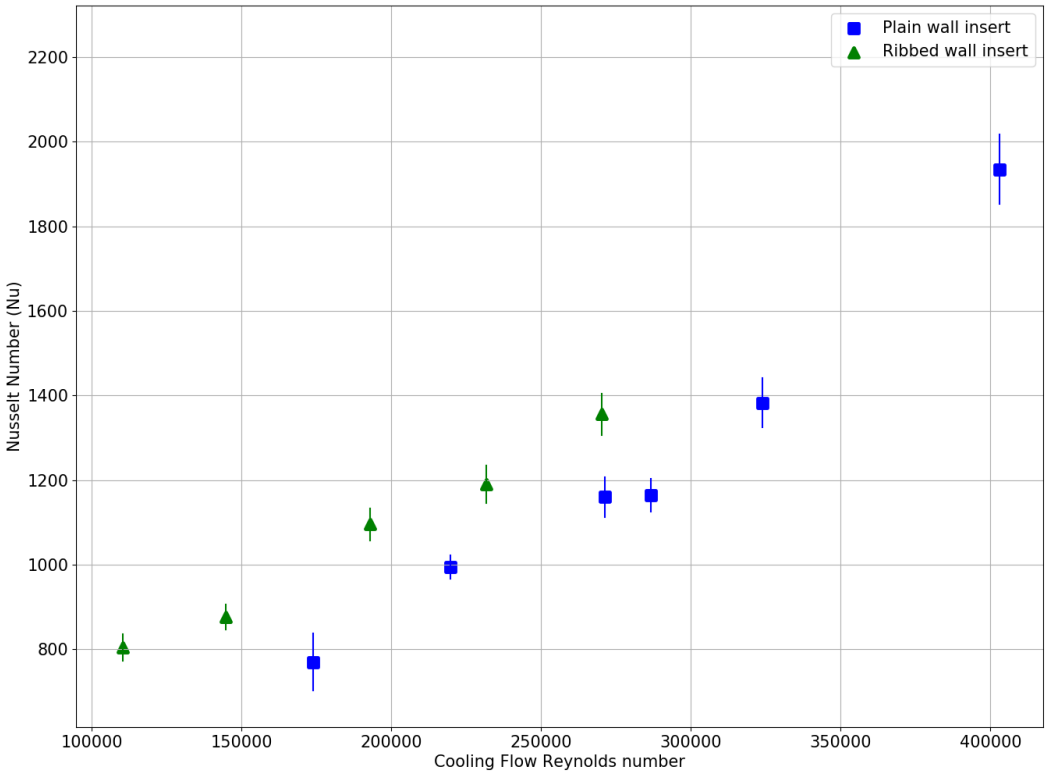

Figure 8. Cooling flow processed Nusselt number for plain and ribbed wall inserts.

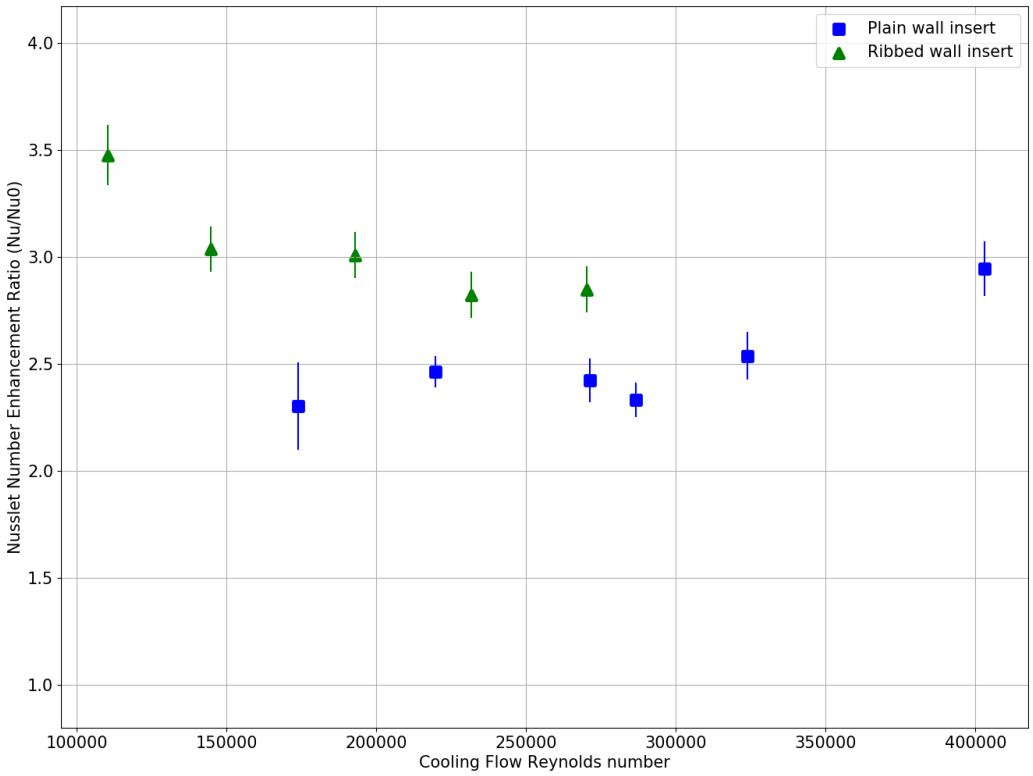

Figure 9. Nusselt number enhancement ratio evaluated for plain and ribbed wall inserts. $\mathbf{Nu_0}$ is evaluated from Eq. 10 for a smooth wall.

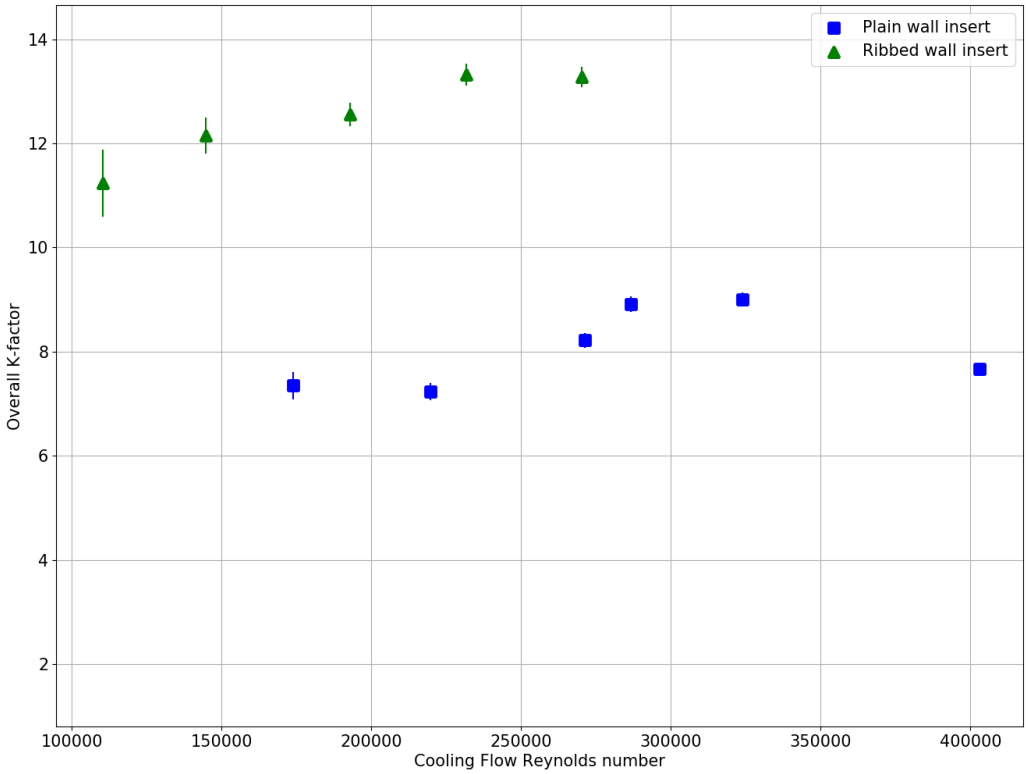

Figure 10. Overall k-factor evaluated for plain and ribbed wall inserts as expressed in Eq. 11.

Two expected trends can be identified from Figure 7 for thermal resistance of the two inserts. For both inserts, the thermal resistance decreases with increasing Reynolds numbers which agrees with the positive correlation between Nusselt number and Reynolds number seen in turbulent flow correlations. The ribbed insert demonstrated lower thermal resistance at test points at similar Reynolds number compared to the plain wall insert. This demonstrates the predicted effect of chevron ribs generating turbulence and increased flow mixing, thereby increasing heat transfer and registering the lower fluid thermal resistance relative to the plain wall. The aforementioned trends are evident as well in the calculated Nusselt numbers (Figure 8). For the Reynolds number range between 150,000 and 300,000 where at least three test points were registered for both inserts, the ribbed wall data points average a Nu/Nu_0 of 2.90 while the plain wall data points have an average of 2.39. These values indicate that though the ribs are the source of a comparatively higher Nusselt enhancement ratio, the plain wall still registers a significantly higher Nusselt number compared to a smooth wall calculation. This is anticipated to be due to the inherent surface roughness of the machined flow path, and also the effect that the 180 deg. tip turns have in promoting turbulence. As expected, the additional enhancement of the ribbed wall geometry came with significantly greater pressure loss due to phenomena including the periodic separation from each rib. The data for the effective k-factor in Figure 10 was produced using Eq. 11, and includes both the frictional losses through each serpentine pass as well as the loss contribution at the tip turns. When using Eq.12 to compensate for an assumed loss factor of 1.5 times the dynamic pressure at each tip turn, f/f_0 for the ribbed wall insert ranges between 5.9 at the lowest Reynolds number and 9.8 at the highest Reynolds number.

CONCLUSION

The heat transfer experiments provide functional quantitative data to the designer of a cooled turbine blade for direct-fired sCO_2 power cycle application. When predicting heat transfer characteristics for midsection ribbed, serpentine internal cooling passages, Nusselt number enhancement ratios near 3 can be expected based on the test data generated at pertinent Reynolds numbers for sCO_2. It is hypothesized that this outcome from the testing was due in a significant part to the inclusion of multiple tip turns through a serpentine path geometry. The geometry is representative of the true blade geometry and the tip turn effect is expected to be prominent for the relatively low length-to-diameter ratio of first stage blade internal passages. Friction factor ratios of up to 10 can be expected for a chevron ribbed passage with characteristics aligned with those enumerated in Table 1, with the exact values depending on the relative losses of the straight passage and due to tip turns. It is important to note there are at least a couple factors that make a sCO_2 turbine different than a gas turbine when considering the impact of internal cooling passage pressure loss. Due to the large pressure difference across the first stage blade for a sCO_2 turbine in direct-fired application, a significant pressure differential is accessible between the internal cooling flow pressure and the external flow path pressure. Second, due to the high density of sCO_2 there can be a significant increase in total pressure for flow through an internal cooling passage traveling from hub to tip due to blade rotation (pumping effect). Both factors may make it the case that less penalty should be ascribed to the pressure losses for internal cooling geometry relative to a gas turbine. While the heat transfer performance data generated is for the overall performance of multiple serpentine passes, for a detailed blade design it becomes important to capture local variation in heat transfer characteristics to better estimate maximum metal temperatures and the resulting impact on material creep life. Future testing is planned for the actual first stage blade while reusing test apparatus components, in order to capture this variation in local external metal temperature and compare it to predictions using the data generated from the present work.

ACKNOWLEDGEMENT

This material is based upon work supported by the U.S. Department of Energy under Award Number DE-FE0031929.

DISCLAIMER

REFERENCES

[1] Weiland, N.T., & White, C.W. (2019). *Performance and Cost Assessment of a Natural Gas-Fueled Direct sCO2 Power Plant*. NETL-PUB-22274. https://doi.org/10.2172/1503567.

[2] 8 Rivers Capital. *Allam Cycle Zero Emission Coal Power: Design Basis, Final Report*. Reference Number 89243319CFE000015.

[3] Wardell, R., Richardson, J., Otto, M., Smith, M., Fernandez, E., Kapat, J. (2023). "An Experimental Investigation of Heat Transfer for Supercritical Carbon Dioxide Cooling in a Staggered Pin Fin Array". *Proceedings of the ASME Turbo Expo 2023: Turbomachinery Technical Conference and Exposition.* GT2023-103263.

[4] Richardson, J., Wardell, R., Fernandez, E., Kapat, J.S. (2023). "Experimental and Computational Heat Transfer Study of sCO_2 Single-jet Impingement". *Proceedings of the ASME Turbo Expo 2023: Turbomachinery Technical Conference and Exposition.* GT2023-102544.

[5] Wright, L.M., Fu, W.L., Han, J.C. (2004). "Thermal Performance of Angled, V-Shaped, and W-Shaped Rib Turbulators in Rotating Rectangular Cooling Channels (AR=4:1)". *ASME Journal of Turbomachinery*. Vol. 126, pp. 604-614.

[6] Wieler, M., Woerz, B., Jeschke, P., Rabs, M. (2019). "Thermal Performance of Angled, V-Shaped, and W-Shaped Rib Turbulators in Rotating Rectangular Cooling Channels (AR=4:1)". *ASME Journal of Turbomachinery*. Vol. 126, pp. 604-614.

[7] Han, J.C., Dutta, S., Ekkad, S. (2013). *Gas Turbine Heat Transfer and Cooling Technology, 2nd Edition.* Section 4.2.10. CRC Press.

[8] Searle, M., Roy, A., Black, J., Straub, D., Ramesh, S. (2021). "Investigating Gas Turbine Internal Cooling Using Supercritical CO_2 at High Reynolds Numbers for Direct Fired Applications". *Proceedings of the ASME Turbo Expo 2021: Turbomachinery Technical Conference and Exposition.* GT2021-59630.

[9] Wilkes, J., Robinson, K., Wygant, K., Pelton, R., Bygrave, J. (2022). "Design and Testing of a 275 bar 700 degree Celsius Expander for an Integrally Geared Supercritical CO2 Compander". *Proceedings of the ASME Turbo Expo 2022: Turbomachinery Technical Conference and Exposition.* GT2022-83284.

[10] Moore, J., Cich, S., Day, M., Allison, T., Wade, J., Hofer, D. (2018). "Commissioning of a 1 MWe Supercritical Test Loop". *Proceedings of the 6th International Supercritical CO_2 Power Cycles Symposium.*

[11] Rau, G. Cakan, M., Moeller, D., Arts, T. (1996). "The Effect of Periodic Ribs on the Local Aerodynamic and Heat Transfer Performance of a Straight Cooling Channel". *Proceedings of the International Gas Turbine and Aeroengine Congress & Exposition.* 96-GT-541.

[12] Chandra, P.R., Niland, M.E., Han, J.C. (1996). "Turbulent Flow Heat Transfer and Friction in a Rectangular Channel with Varying Number of Ribbed Walls". *Proceedings of the International Gas Turbine and Aeroengine Congress & Exposition.* 95-GT-13.

[13] ASME. (2013). ASME Boiler and Pressure Vessel Code Section VIII-Rules for Construction of Pressure Vessels. New York.

[14] Incropera, F.P., Dewitt, D.P., Bergman, T.L., Lavine, A.S. (2007). *Fundamentals of Heat and Mass Transfer, 6th ed*. John Wiley & Sons.

[15] ASME International. “Policy on Reporting Uncertainties in Experimental Measurements and Results”. Journal of Heat Transfer Policy.